Full Text View

Volume 32, Issue 6 (June 2002)

Journal of Physical Oceanography
Article: pp. 1621–1641 | Abstract | PDF (1.43M)

Low-Frequency Current Observations in the Korea/Tsushima Strait*

W. J. Teague, G. A. Jacobs, H. T. Perkins, and J. W. Book

Naval Research Laboratory, Stennis Space Center, Mississippi

K.-I. Chang and M.-S. Suk

Korea Ocean Research and Development Institute, Seoul, Korea

(Manuscript received March 13, 2001, in final form September 21, 2001)

DOI: 10.1175/1520-0485(2002)032<1621:LFCOIT>2.0.CO;2

ABSTRACT

High resolution, continuous current measurements made in the Korea/Tsushima Strait between May 1999 and March 2000 are used to examine current variations having time periods longer than 2 days. Twelve bottom-mounted acoustic Doppler current profilers provide velocity profiles along two sections: one section at the strait entrance southwest of Tsushima Island and the second section at the strait exit northeast of Tsushima Island. Additional measurements are provided by single moorings located between Korea and Tsushima Island and just north of Cheju Island in Cheju Strait. The two sections contain markedly different mean flow regimes. A high velocity current core exists at the southwestern section along the western slope of the strait for the entire recording period. The flow directly downstream of Tsushima Island contains large variability, and the flow is disrupted to such an extent by the island that a countercurrent commonly exists in the lee of the island. The northeastern section is marked by strong spatial variability and a large seasonal signal but in the mean consists of two localized intense flows concentrated near the Korea and Japan coasts. Peak nontidal currents exceed 70 cm s^{-1} while total currents exceed 120 cm s^{-1}. The estimated mean transport calculated from the southwest line is 2.7 Sv (Sv $\equiv 10^6$ m^3 s^{-1}). EOF analyses indicate total transport variations in summer are due mainly to transport variations near the Korea coast. In winter, contributions to total transport variations are more uniformly distributed across the strait.

1. Introduction

- J. W. Book
- K.-I. Chang
- M.-S. Suk

Of the four straits that connect the Japan/East Sea with adjacent seas (Korea, Tsugaru, Soya, and Tatar Straits), the Korea/Tsushima Strait provides the vast majority of inflow and thus is instrumental in controlling the Japan/East Sea properties. The major influx of seawater entering the Japan/East Sea through this strait is important in the transfer of dynamic, thermodynamic, biological, and passive tracer properties into the Japan/East Sea. This strait is effectively a shallow, connecting channel between the broad, shallow East China Sea (depths of approximately 50 to 1000 m) and the much deeper Japan/East Sea (depths exceed 2000 m). Korea/Tsushima Strait is about 330 km long and 100 m in depth. The strait is about 160 km wide and is divided by Tsushima Island into the East and West channels. The western channel contains a closed topographic depression in its center, approximately 60 km long, 10 km wide, and maximum depth 200 m. Its position is approximated in Fig. 1 by the 150 m closed contour west and northwest of Tsushima Island.

Long-term measurement of currents in the Korea/Tsushima Strait are very difficult to acquire due to the intense level of fishing and trawling (Kawatate et al. 1988). Hence, such measurements are relatively scarce. Many short-term current measurements have shown strong currents in addition to strong tidal components (Mizuno et al. 1989; Egawa et al. 1993; Isobe et al. 1994; Katoh et al. 1996). The major current features in the strait are the inflow of the warm Tsushima Current from the East China Sea, the outflow into the Japan/East Sea, and a counterflow on the east side of Tsushima Island (Miita and Ogawa 1984; Egawa et al. 1993). The current direction is generally northeastward along the channel, but southwestward countercurrents have been observed (Katoh 1994; Isobe et al. 1994). Tidal currents with speeds approaching 50 cm s^{-1} embedded in total currents of nearly 100 cm s^{-1} have been reported in the strait by Isobe et al. (1994).

Currents in the strait are generally thought to exhibit considerable seasonal variation in current velocity (Egawa et al. 1993). Due to the scarcity of long-term direct current measurements, particularly in the winter season, this variability has been deduced from seasonal variations in water mass properties and in the sea level differences among tidal stations along the Korean and Japanese coasts. Many of the direct current measurements are made using ship-mounted acoustic Doppler current profilers (ADCPs) where removing ship motions and tides are often a large source of error. Large seasonal variation in the currents (higher magnitudes in the summer than in the winter) have been deduced using the geostrophic current calculation (Yi 1966) and the sea level differences (Yi 1970; Kawabe 1982; Toba et al. 1982). According to these studies, currents are at a maximum in summer–fall and at a minimum in winter–spring in the western channel. However, similar studies in the eastern channel have found little seasonal variability (Isobe et al. 1994). Egawa et al. (1993) analyzed ship-mounted ADCP observations taken over a three-year period. They found that the main axis of the Tsushima Current exists in the channel west of Tsushima Island for all seasons and that the current flowing east of Tsushima Island is slower than the current in the western channel but also is present during all seasons. Little seasonal variation is observed but largest current speeds are observed in October through December time period with maximum currents in the near-surface layer in December and at middepth in November.

The development of trawl resistant mounts for mooring instruments on the bottom makes long-term measurements possible in the strait. This technique was used in the Yellow Sea to deploy ADCPs and pressure gauges (Teague et al. 1998; Teague and Jacobs 2000). This study analyzes data from 14 similar moorings in the strait (Fig. 1). Most of these moorings were deployed for about ten months. Twelve of the moorings (N1–N6, S1–S6) are located on sections nearly spanning the strait to the northeast and southwest of Tsushima Island. The other two moorings are located just north of Cheju Island and between Korea and Tsushima Island. One purpose of these measurements is to delineate the nontidal currents and thus gain a better understanding of the dynamics in the strait. Using the first five months of these measurements, Perkins et al. (2000a) present a short description of the current flow, and Jacobs et al. (2001b) estimate transports of 2.5 and 2.9 Sv (Sv $\equiv 10^6$ m^3 s^{-1}) through the northeastern and southwestern lines, respectively. Along the southwestern section, nontidal flows exceed 50 cm s^{-1}, and along the northeastern section nontidal flows exceed 70 cm s^{-1}. The two sections show markedly different flow regimes. At the southern entrance the flow through the strait contains a broad maximum at midchannel. The northeastern section, is marked by strong spatial variability, but in the mean consists of two streams, one on each side of the strait. Between the two is a regime of highly variable flow with a weak mean, presumably due to the separation of the flow by Tsushima Island. Tides are found to significantly contribute to the total current flow and are described by Teague et al. (2001). Total currents with tides can be twice as large as the currents without tides. Inertial currents dynamics within the strait, particularly important during summer, are examined by Jacobs et al. (2001a).

Numerous studies have proposed different theories on the dynamics of the generation mechanism and seasonal variation of the Tsushima Current. The low frequency current variations are expected to be mainly related to the sea level drop between the East China Sea and the Japan/East Sea and ultimately linked to the meridional sea level difference between the inflow and outflow ports (Ohshima 1994). Height differences across the strait are due to local wind stress, remote wind stress across the adjoining seas, and steric variations. In addition, the large-scale circulation in the Pacific Ocean influences the sea level in the East China Sea and the sea level at the outflow through Tsugaru Strait, and hence the sea level within the Japan/East Sea (Nof 2000). Local wind forcing (Huh 1982) and local stratification (Sekine 1988) due to the intrusion of

bottom cold water (Isobe 1997) are also important in the seasonal variation of the Tsushima Current. The forcing and dynamics that lead to variations examined here are complex. Within this study, we only address the characteristics of variations and nature of the low frequency flow.

Current profiles measured by bottom moored ADCPs over long time periods are ideal for answering questions pertaining to the currents and tides that have never been adequately addressed due to the difficulty in making such measurements. Several error sources are mitigated by the measurements. Namely, spatially sparse measurements using single moorings provide poor coverage, and ship ADCP sections can be biased by short time period events. However, caution should be exercised in interpreting the results since the data reflects variability only through the one deployment time.

2. Instrumentation

A technique for mooring ADCPs on the bottom in areas of high fishing activity was recently developed. This method utilizes dome-shaped mounting pods, which are highly trawl resistant (Cumbee and Foley 1995). The U.S. Naval Oceanographic Office implemented similar moorings in 1995 in the Yellow Sea (Teague et al. 1998). Within the Korea/Tsushima Strait, 14 mooring packages were deployed in a combined effort between the Naval Research Laboratory, the Naval Oceanographic Office, and the Korea Ocean Research and Development Institute (KORDI). Six moorings were deployed along each of two sections that span the entire Korea/Tsushima Strait. One section is located northeast of Tsushima Island (mooring positions denoted by N1–N6 in Fig. 1) and the other is located southwest of Tsushima Island (denoted by S1–S6 in Fig. 1). The deployment times generally cover the period from May 1999 through March 2000. Moorings along the two sections were recovered and redeployed in October 1999. Addition moorings were deployed in the strait between Tsushima Island and Korea (C1) from October 1999 through March 2000 and in Cheju Strait (K1) from March 1999 through December 1999. Geographical positions, deployment periods, water depths, and ADCP sample levels are provided in Table 1.

Each deployed package consists of an ADCP and a wave/tide gauge (except at C1 and K1) housed in a trawl-resistant bottom mount (TRBM). Nine of the deployments are based on a new type of TRBM known as Barnys after their barnacle-like shape (Perkins et al. 2000b). The Barnys were developed by SACLANT Center in Italy in collaboration with the Naval Research Laboratory (NRL). The remaining TRBMs, at sites C1, N2, N3, and S5, are of a design developed at the Naval Oceanographic Office (Teague et al. 1998). The mooring at K1, deployed by KORDI, consists of a commercially available TRBM. In general, these types of mounts are shallow dome-shaped enclosures that rest upon the bottom. The exposed side of the dome is relatively smooth in order to minimize snagging by fishing nets and lines. Scraps of nets as well as evidence of trawl scrapings were found on the moorings at instrument retrieval. There was no evidence of adverse impact on the data records due to fishing activities.

The Barny mounts and the commercial mount are equipped with RD Instruments Workhorse ADCPs operating at 300 KHz. The TRBMs from the Naval Oceanographic Office are equipped with RD Instruments Narrowband ADCPs operating at 150 KHz. Most of the packages contain Sea-Bird Electronics Model 26 wave/tide gauges and all contained EdgeTech Model 8202 acoustic releases for location and recovery. The instruments, protected within the mount, rest about 0.5 m above the ocean bottom. The ADCPs are set up to provide current profiles with an accuracy of 1 cm s^{-1} over nearly the full water column. Vertical resolution was set to 4 m, except at S1, S2, and N2 where resolution was set to 2 m. Profiles of U (east–west) and V (north–south) components of velocity are recorded at 30-min intervals except at 15-min intervals at S5, N2, and N3.

For analyses of the low-frequency current, tidal currents and currents near the tidal semidiurnal and diurnal frequencies are removed from the ADCP records by using a low-pass filter with a 40-h cutoff frequency. Velocities are then rotated (42.5°) such that the V_r component is approximately along strait, normal to the ADCP section, and U_r is cross strait, approximately parallel to the section.

3. Snapshots

An overview of along-strait current velocities is provided in snapshots shown in Figs. 2 and 3. Velocities are interpolated along the northeast and southwest section after tide removal to provide two-dimensional pictures or snapshots of the flow using the optimal interpolation described in Jacobs et al. (2001b). Snapshots of the velocities for components normal to each section (V_r) are shown for representative current configurations (approximately 10 days apart) in Fig. 2 for the southwestern section. A high velocity core with peak velocities greater than 30 cm s^{-1} are observed along the western bathymetric slope of the south section for the entire 10-month period. The high velocity core sometimes extends to the bottom. Another high velocity core is infrequently observed on the eastern bathymetric slope in the upper half of the water column, sometimes not extending to the surface layers. Current flow toward the southwest is sometimes observed on the northeastern and southwestern ends of the section near land boundaries.

Snapshots of the velocities for the northeastern section are shown in Fig. 3. High velocity currents directed toward the

northeast are frequently observed near both ends of the section. They can extend from the surface to near the bottom or can take the form of a subsurface jet. Current flow near the middle portion of the north section is sometimes relatively weak toward the northeast. However, there is often a counterflow toward the southwest that can extend from the surface to the bottom. Such a current configuration, as on 9 October, has been depicted by Miita and Ogawa (1984) using geostrophic current calculations and short-term current meter measurements. The deep countercurrent in the depression on the northwestern end of the section, such as on 23 August, is associated with the movement of cold water into the Korea/Tsushima Strait from the Japan/East Sea and has been observed previously (Lim 1973; Kaneko et al. 1991).

4. Velocity distributions

A wide range of velocities are observed in the strait. Nontidal velocities can be in excess of 75 cm s^{-1} at N1, and tides can greatly affect these velocities. Current speed distributions within 10 cm s^{-1} velocity bins, with tides and without tides for near-surface velocities, are shown in Fig. 4. When tides are included speed distributions generally appear more Gaussian, and speeds can nearly double. For example, at C1 during the entire October 1999 through March 2000 recording period, largest low-frequency currents are observed in the 70–80 cm s^{-1} velocity bin while largest total currents (with tides) are observed in the 160–170 cm s^{-1} velocity bin. Inclusion of tides significantly affects the speed distributions, particularly at the low and high speed ends of the distributions. Current speeds can reach 100 cm s^{-1} throughout the strait.

Low speeds (0–10 cm s^{-1} bin) for the low frequency currents dominate at the ends of the southwestern section (S1, S6) and often at the highly variable N3 and N4 locations. Higher speed distributions occur in the middle of the southwestern section and at the ends of the northeastern section. Low frequency current speeds are generally smallest in January through March and highest in October and November. Over the entire recording periods, speed distributions are similar between K1 and S2, C1 and N1, N3 and N4, and N5 and N6.

5. Vertically averaged currents

Current flow in the interior of the strait generally follows the bathymetry contours (Lie et al. 1998). Because much of the flow and its associated variability is to the northeast, the V_r component reflects most of the signal. The exception to this rule occurs at N3 and N4, located downstream of Tsushima Island in an area of weak flow and relatively isotropic variability.

Vector stick diagrams of current velocities averaged over depth and sub sampled at 6-h intervals are presented in Fig. 5. Current flow is predominately toward the northeast except at moorings N3, N4, and S6 where direction is highly variable. However, isolated southwestward flow events occur at each of the moorings. Current characteristics appear to vary over timescales ranging from several days to about a week. Maximum velocities, exceeding 60 cm s^{-1}, are observed at N1.

Along the southwestern section (Fig. 5b), current flow increases to a broad maximum at midchannel, with current speeds of about 50 cm s^{-1}. Large, northeastward velocity components are dominant at S2, S3, and S4, with the largest velocities at S3. Velocities are weaker at S1 and S6. Velocities at K1 in Cheju Strait are stronger than those at S1 but a little weaker than those at S2. Sporadic countercurrents or southwest flows are observed along both ends of the southwestern section at S1, S2, and S6. The strongest southwest flow burst along the south section occurs near day 265 at S1, S2, and K1, exceeds 20 cm s^{-1}, and has a duration of over a week. This burst is associated with Super Typhoon Bart's passage.

Along the northeastern section (Fig. 5a), strongest northeast flows (V_r) are observed at the ends of the section at N1 and N2, and at N5 and N6. Currents are much weaker near midstrait at N3 and N4 and reverse direction frequently. Flow reversals due to the effects of Bart are apparent at N2, N3, and N4. All of the moorings on the northeastern section exhibit at least some southwestward flow into the strait from the Japan/East Sea. Strong northeastward flow at C1 appears similar to the flow at N1.

6. Monthly variability

An overall picture of the current field can be gained from mapping the currents averaged over the year at each of the moorings for several depth levels. Mean currents for the entire 11-month period at depth levels near the surface, at middepth, near the bottom, and for vertically averaged currents with standard deviation ellipses are shown in Fig. 6. The center of the standard deviation ellipse is at the tip of the arrowhead and reflects the area that is within one standard deviation of the mean. Mean directions appear to closely follow the bathymetry at the southwestern section with the possible exception of S1 where local bathymetry effects may be significant. Flow at S1 is northward toward the Korea coast. The strongest currents have means much larger than their respective deviation ellipses. Therefore, the best determined depth-averaged currents are at S3, C1, and N1. The strongest mean currents occur on the western side of the strait. Mean current directions along the northeastern section flow to the northeast except for the weaker currents observed at N3 and N4 and

the near-bottom currents at N1 and N2, which are directed toward Korea. Largest variability, indicated by the major axes of the standard deviation ellipses, generally appears in the direction of the mean flows.

The mean current vectors and their standard deviation ellipses are shown for individual months for near-surface, middepth, and near-bottom levels in Figure 7. These vectors are similar to those shown in Fig. 6 but are not on a geographical grid for illustrative purposes. Stronger and more persistent flows are observed in the interior of the strait along the southwestern section. Currents tend to be more variable and weaker near the coasts. Very small near-bottom flows are observed at K1 and S6. A southwestern mean flow in all three layers is found for February at S1.

Along the northeastern section largest monthly mean currents are found near Korea (N1 and N2). Mean currents at N3 and N4 tend to be much weaker and more variable in direction than at any other location. Occurrences of southwestward currents are common. Elsewhere along the northeastern section currents are almost always toward the northeast and show a more pronounced seasonality with stronger flows in summer and fall. Near-bottom mean southwestward currents into the strait are only observed at N1 in January, opposite to the general northeastward flow.

A seasonal signal consisting of larger mean velocities during the summer and fall months is apparent in the near-surface layers. Variability is also correspondingly larger. Seasonality appears to be more pronounced along the northeastern section than along the southwestern section. Seasonality is reduced below the surface layer, and seemingly more so along the southwestern section than along the northeastern section. Although mean currents are small at S6, a striking seasonality is evident in the near-surface layer with countercurrents observed from October to February. Along the northeastern line, largest near-bottom mean velocities occur near the ends of the line (N1, N2, and N6) during spring months. The large mean flow in October at N1 is based only on about one week of data. Larger standard deviation ellipses occurring in September are likely associated with the passage of Typhoon Bart.

Mean velocity profiles for the U_r (cross-strait) and V_r (along-strait) components with standard deviations are shown in Figs. 8a and 8b. Larger velocities are clearly in the along-strait direction and near the surface. Largest monthly mean velocity, exceeding 60 cm s^{-1}, is found at N1 in November. Mean velocities exceeded 70 cm s^{-1} over the single week of data recorded at N1 in October. Mean velocities of about 55 cm s^{-1} are observed at C1, located between Tsushima Island and Korea.

The mean profiles generally reflect current flow through the strait from the Yellow and East China Seas and into the Japan/East Sea. Profiles of V_r at C1 appear to mirror profiles observed at N1. Flow at K1 is qualitatively similar to the flow at S2. There are a number of cases (at S1, S6, N1, N3, and N4) where the mean velocities reflect a counterflow. The counterflow occurs throughout the mean profile at S1 in February and at S6 in December.

The countercurrent that bifurcates from the eastern side of the Tsushima Current along the southeastern end of the section, near the west coast of the Goto Islands, has also been observed by Katoh et al. (1996) using ship mounted ADCP instrumentation. The frequency of this countercurrent was unknown. The measurements here at S6 show a monthly mean southward flow in the winter and spring that is more pronounced in the near surface. Variability in the current is such that a southerly flow is commonly observed during all months of the year.

Overall variability is generally larger for the along-strait component along the northeastern line. As expected, mean velocities are much larger for the along-strait component. Currents become more nearly barotropic during the winter months.

7. Transport

Transport variations across the strait are computed (Fig. 9) by vertically integrating the interpolated velocity sections as computed by Jacobs et al. (2001b). The high velocity core, centered at about 120 km off Korea, is apparent in the southwestern section. Southwestward flow reversals are apparent at about 80 km off Korea along the northeastern section and near the ends of the southwestern section. Seasonality is most pronounced at the end of the northeastern section closest to Korea. Transport is higher in the channel west of Tsushima Island in October and November than in the eastern channel. Transport estimates for both sections are presented as a function of time in Fig. 10. Transports previously estimated by Jacobs et al. (2001a,b) for May through October 1999 are 2.9 Sv through the southern section and 2.5 Sv through the northern section with expected errors of about 0.5 Sv. The time-averaged transports for May 1999 through March 2000 are 2.7 Sv across the southwestern section and 2.3 Sv across the northeastern section, with standard deviations of about 0.9 for both lines.

The transport estimate for the northeastern section is 0.4 Sv smaller than the estimate for the southwestern section. There are several reasons that may lead to transport not observed through the northeastern section. Typical scales observed are between 15 and 30 km. However, narrow currents not resolvable by the moorings along the section could exist. High-resolution snapshots of currents across the strait obtained by a ship-mounted ADCP (Isobe et al. 1994) indicate currents

more narrow than the mooring spacing do occur. In addition, high velocity currents are also known to exist near the Korea Coast that decrease away from the coast (Miita and Ogawa 1984; Egawa et al. 1993). These currents are not resolved by the northeastern section. Thus the northeastern section would underestimate the transport if either an intensified coastal current or narrow currents between moorings exist. Finally, it is possible that the velocity field becomes surface intensified. The measurements do not resolve the near-surface layer. Thus, surface intensification could also play a role in the smaller observed transport along the northeastern section.

Short-term transport variations appear to occur on timescales of three days to one week. Long-term transport variations seem to steadily increase from about 1 Sv in December to about 4 Sv in October, and then begin to decrease rapidly in November. Monthly mean transports are given in Table 2. Maximum monthly mean transports are observed in October and minimum transports in January.

8. Spectra

Energy spectra are computed from near-surface velocity measurements for the northeast and southwest sections (Fig. 11). Spectral estimates from 30-day segments of velocity data sampled at 1-h intervals are averaged for all moorings along each section. Spectra for the along-strait velocity (V_r) are shown for each section for summer (May–mid October) and winter (mid October–March). Overall energy levels are higher along the northeast section than along the southwest section for periods longer than 2 days (0.5 cpd). Energy levels are higher along both sections during winter for periods from about two days to a week. The higher energies are likely associated with more energetic wind events during winter. Wind pulses that have durations of about a week are commonly observed in this region. Marginally significant peaks in the spectra for the northeast section occur for both summer and winter for frequencies associated with periods between 6 and 7 days. Peaks also occur along the southwest section near these frequencies. The peaks at 1 and 2 cpd are due to tides (Teague et al. 2001).

The peaks at about 1.1 cpd, present only during the summer for both sections, are associated with inertial currents. There is a strong inertial oscillation response to wind stress in summer and a much weaker response in winter, even though wind events are comparable in both seasons. Inertial oscillations within the Korea/Tsushima Strait indicate a vertical velocity structure in which the velocity reverses direction near the depth of the mixed layer in summer. Strong summer stratification prevents wind stress momentum flux from mixing downward and allows for a surface flow toward the coasts with a subsurface return counterflow. The lack of stratification in winter does not allow for such development of inertial currents. Inertial currents in the Korea/Tsushima Strait are fully described by Jacobs et al. (2001a).

9. EOF analysis

The variance ellipses (Fig. 7) indicate the primary directions of velocity variability for individual depth levels for each ADCP. However, these ellipses alone do not provide an indication of how velocity variations may be related between different depths and between moorings. Jacobs et al. (2001b) provide the horizontal and vertical decorrelation scales at each velocity level for the ADCPs along the northeast and southwest sections. The horizontal length scales vary from 20 to 40 km with a slight decrease at the thermocline depth. Vertical scales vary from 10 m near the surface to 20 m near the bottom. The spatial separation of the moorings is slightly less than the observed decorrelation scales.

To examine the main correlation patterns within the ADCP datasets (northeast and southwest sections, only), the observations are decomposed by an empirical orthogonal function (EOF) analysis (Preisendorfer 1988). The analysis is carried out separately for the observations in summer (May through August) and winter (November through March) since the wind forcing and ocean stratification are significantly different during these two time periods. September is excluded from the analysis because of an anomalously large event on day 260. This event is the ocean response to Super Typhoon Bart that passed from the southwest across Kyushu. This single event can bias the covariance statistics and result in a biased view of the typical correlations between ADCPs. Each time series of u and v is detrended over the separate time periods to examine the interrelations at timescales on the order of 1 month or less.

Only the first two EOFs for winter and summer are examined. The first summer EOF (Fig. 12a) indicates most of the velocity variability near the Korean coast at moorings S1, S2, N2, and N3. The velocity variations are to the northeast (when the time series amplitude is positive) and southwest (when the time series amplitude is negative), and the variations are surface intensified. The time series indicates timescales of 5 to 7 days. The overall impression from this first mode is that the summer transport variations in the strait are primarily due to strengthening and weakening of the flow on the Korea side of the strait. This first summer EOF mode explains 18.8% of all the variability at all depths of all the ADCPs located on the northeast and southwest sections. The second summer EOF mode (Fig. 12b) explains 15.8% of the variability and is composed mainly of variability along the northern mooring line. This indicates a shifting of the strait outflow between the Nearshore Branch and the East Korea Warm Current.

The winter EOF decomposition (Fig. 12b) indicates more barotropic variability compared to summer. This would be expected since the winter density structure is nearly constant over depth while the summer density structure contains a

sharp pycnocline at depth 30 to 40 m. The first EOF mode indicates variability in the along-strait direction that is relatively constant with depth. The directions of the vectors across most of the south mooring line are similar. The north mooring line also indicates variations that are relatively constant over depth, and the velocity variations near the Korea and Japan coasts are in the same direction as those along the south line. However, at N3 and N4 in the center of the north line the velocity variations are small and nearly in opposite direction to the other ADCPs. The implication is that the winter transport variations are due to homogeneous currents across the strait except in the lee of Tsushima Island. The second winter EOF (Fig. 12b) contains a large divergence on the north line between N1 and N2 and a large convergence between N3 and N5. The flow along the south line does not seem to play a large role in this variability.

10. Summary and conclusions

A persistent main velocity core of along-strait current flow through the southwestern Korea/Tsushima Strait lies along the bathymetric slope on the western side of the strait. The single current core apparent in the southwestern section separates into two branches near the Japan and Korea coasts as it splits around Tsushima Island before reaching the northeastern section. In the lee of Tsushima Island, the two branches are separated by a region (sites N3 and N4) where currents are variable and lack a well-defined mean. Based only on these data, we conclude that the single current core found upstream is divided by its passage around Tsushima Island and that the band of variability is an island-induced effect. It is well established that flow from the strait eventually takes two divergent paths in the Japan/East Sea. One branch, the East Korean Warm Current, flows northward along the eastern coast of Korea. The second branch (the Nearshore Branch) flows eastward along the northern coast of Japan. However, the point at which these two currents bifurcate is not well established (Kaneko et al. 1991; Katoh et al. 1996). We presume that the two streams apparent at our northern mooring line are an expression of this separation at Tsushima Island. Profile variability in U_r at N1 (Fig. 8a) points toward a northward flow up the coast of Korea. However, once this flow has passed the steep bathymetric drop-off at the entrance to the Japan/East Sea, it is expected that a further bifurcation occurs and that two branches become dynamically separated (Katoh 1994). The branches are constrained to follow bathymetric contours. Another possible flow scenario suggested by Kim and Legeckis (1986) is the occasional absence of the East Korean Warm Current. Instead, the flow through the western channel of the Korea/Tsushima Strait forms an offshore branch along the Japanese coast following the continental slope, while the Nearshore Branch on the continental shelf is fed by the flow through the eastern channel (Hase et al. 1999). The absence of the East Korean Warm Current is attributed to the development of the southward movement of Korea/Tsushima Strait bottom cold water (Cho and Kim 2000).

Interannual variations are unknown and could cause significant departures from this one measurement of the seasonal flow. Seasonality in the currents along the southwestern section is weak. Near-surface layer currents along the northeastern section are larger and usually more highly variable in the summer and fall months (Fig. 7a). Flows at middepths are smaller and less variable but similar to the near-surface flows along both sections (Fig. 7b). Very little seasonality is observed near the current core at middepth at S3. Flows near the bottom are smaller but similar to those at middepth (Fig. 7c) except at N1, N2, and N6 where the larger velocities are found during the spring season. A more concentrated outflow along the northeastern section could magnify smaller variability in the main velocity core observed along the southwestern section. EOF analyses indicate that the seasonality may be driven by current variability on the Korea side of the strait. The first two EOF modes explain about 35% of the variability.

The downstream transformation of the Tsushima Current due to the confluence of Cheju Strait and East China Sea waters and the subsequent bifurcation of current into the eastern and western channels of the strait is still poorly understood. The flow through Cheju Strait passes mostly through the western channel of the Korea/Tsushima Strait (Lie et al. 2000), and constitutes about 30% of the total transport through the western channel of the Korea/Tsushima Strait (Chang et al. 2000). Through combined analyses of hydrographic and ship-mounted ADCP measurements Katoh et al. (1996) concluded that the substantial bifurcation of the Tsushima Current occurs in the vicinity of Tsushima Island. The measurements here cannot determine where the current bifurcation occurs. If the flow follows the bathymetry (Fig. 1), then flow through S1–S4 would pass west of Tsushima Island. However, the mean flow directions suggest that the flow through S1, S2, and S3 continues on west of Tsushima Island while the flow at S4, S5, and S6 continues on east of Tsushima Island (Fig. 6). Nontidal velocity distributions at S3 are more similar to the distributions at C1 than the velocity distributions at S4 (Fig. 4). These velocity distributions also suggest a split between S3 and S4. The monthly mean flow at S4 is always more eastward than the mean current direction at S3. Such a flow pattern would correspond to a larger transport on the western side of Tsushima Island and is consistent with transports reported by Kaneko et al. (1991) and Katoh et al. (1996). Measurements here show that the transport is larger in the western channel for September, October, and November.

The strongest currents are observed off the coast of Korea and are approximately 100 cm s^{-1} but are nearly 170 cm s^{-1} if tidal current contributions are included. The seasonal flow pattern in the near-surface layer is more pronounced northeast of Tsushima Island than southwest of Tsushima Island. The enhanced seasonal signal may be due to more concentrated outflows near the coasts of Korea and Japan, where most of the current flow into the Japan/East Sea appears to occur. Seasonal patterns become less pronounced at depth. Southwestward flow events are not uncommon near the coasts along the southwestern section and near the middle of the strait along the northeastern section. Mean transport through the strait, observed over the 10 months, is 2.7 Sv with a standard deviation of 0.9 Sv. Transport is minimum in January and increases

to a maximum in October.

Acknowledgments

This work was supported by the Office of Naval Research as part of the Basic Research Projects “Linkages of Asian Marginal Seas” and “Japan/East Sea DRI” under Program Element 0601153N. Chang and Suk were supported by grants from the KORDI's in-house project “Marine Ecosystem Response to Climate Variability in the East Sea and Tectonic Evolution” under Project Number PE00783.

REFERENCES

Chang K.-I., M.-S. Suk, I.-C. Pang, and W. J. Teague, 2000: Observations of the Cheju Current. *J. Korean Soc. Oceanogr.*, **35**, 129–152.

Cho Y.-K., and K. Kim, 2000: Branching mechanism of the Tsushima Current in the Korea Strait. *J. Phys. Oceanogr.*, **30**, 2788–2797. Find this article online

Cumbee S. A., and J. M. Foley Jr., 1995: Naval Oceanographic Office's first operational use of trawl-resistant packages housing acoustic Doppler profilers. *Oceans*, **2**, 1372–1380.

Egawa T., Y. Nagata, and S. Sato, 1993: Seasonal variation of the current in the Tsushima Strait deduced from ADCP data of ship-of-opportunity. *J. Oceanogr.*, **49**, 39–50. Find this article online

Hase H., J.-H. Yoon, and W. Koterayama, 1999: The current structure of the Tsushima Warm Current along the Japanese coast. *J. Oceanogr.*, **55**, 217–235. Find this article online

Huh O. K., 1982: Spring season flow of the Tsushima Current and its separation from the Kuroshio—Satellite evidence. *J. Geophys. Res.*, **87**, 9687–9693. Find this article online

Isobe A., 1997: The determinant of the volume transport distribution of the Tsushima Warm Current around the Tsushima/Korea Straits. *Cont. Shelf Res.*, **17**, 319–336. Find this article online

Isobe A., S. Tawara, A. Kaneko, and M. Kawano, 1994: Seasonal variability in the Tsushima Warm Current, Tsushima–Korea Strait. *Cont. Shelf Res.*, **14**, 23–35. Find this article online

Jacobs G. A., J. W. Book, H. T. Perkins, and W. J. Teague, 2001a: Inertial oscillations in the Korea Strait. *J. Geophys. Res.*, **106**((C11),), 26943–26957. Find this article online

Jacobs G. A., H. T. Perkins, W. J. Teague, and P. J. Hogan, 2001b: Summer transport through the Korea–Tsushima Strait. *J. Geophys. Res.*, **106**, 6917–6929. Find this article online

Kaneko A., S.-K. Byun, S.-D. Chang, and M. Takahashi, 1991: An observation of sectional velocity structures and transport of the Tsushima Current across the Korea Strait. *Oceanography of Asian Marginal Seas*, K. Takano, Ed., Elsevier, 179–195.

Katoh O., 1994: Structure of the Tsushima Current in the southwestern Japan Sea. *J. Oceanogr.*, **50**, 317–338. Find this article online

Katoh O., K. Teshima, K. Kubota, and K. Tsukiyama, 1996: Downstream transition of the Tsushima Current west of Kyushu in summer. *J. Oceanogr.*, **52**, 93–108. Find this article online

Kawabe M., 1982: Branching of the Tsushima Current in the Japan Sea, Part I. Data analysis. *J. Oceanogr. Soc. Japan*, **38**, 95–107. Find this article online

Kawatate K., T. Miita, Y. Ouchi, and S. Mizuno, 1988: A report on failures of current meter moorings set east of Tsushima Island from 1983 to 1987. *Progress in Oceanography*, Vol. 21, Pergamon, 319–327.

Kim K., and R. Legeckis, 1986: Branching of the Tsushima Current in 1981–1983. *Progress in Oceanography*, Vol. 17, Pergamon, 256–276.

Lie H.-J., C.-H. Cho, and J.-H. Lee, 1998: Separation of the Kuroshio water and its penetration onto the continental shelf west of Kyushu. *J. Geophys. Res.*, **103**, 2963–2976. Find this article online

Lie H.-J., S. Lee, and Y. Tang, 2000: Seasonal variation of the Cheju Warm Current in the northern East China Sea. *J. Oceanogr.*, **56**, 197–211. Find this article online

Lim D. B., 1973: The movement of the cold water in the Korea Strait. *J. Ocean. Soc. Korea*, **8**, 46–52. Find this article online

Miita T., and Y. Ogawa, 1984: Tsushima currents measured with current meters and drifters. *Ocean Hydrodynamics of the Japan and East China Seas*, T. Ichiye, Ed., Elsevier, 67–76.

Mizuno S., K. Kawatate, T. Nagahama, and T. Miita, 1989: Measurements of East Tsushima Current in winter and estimation of its seasonal variability. *J. Oceanogr. Soc. Japan*, **45**, 375–384. Find this article online

Nof D., 2000: Why much of the Atlantic circulation enters the Caribbean Sea and very little of the Pacific circulation enters the Sea of Japan. *Progress in Oceanography*, Vol. 45, Pergamon, 39–67.

Ohshima K. I., 1994: The flow system in the Japan Sea caused by a sea-level difference through shallow straits. *J. Geophys. Res.*, **99**, 9925–9940. Find this article online

Perkins H., W. J. Teague, G. A. Jacobs, K.-I. Chang, and M.-S. Suk, 2000a: Currents in Korea–Tsushima Strait during summer 1999. *Geophys. Res. Lett.*, **27**, 3033–3036. Find this article online

Perkins H., F. de Strobel, and L. Gualdesi, 2000b: The Barny sentinel trawl-resistant ADCP bottom mount: Design, testing, and application. *IEEE J. Oceanic Eng.*, **25**, 430–436. Find this article online

Preisendorfer R. W., 1988: *Principal Component Analysis in Meteorology and Oceanography*. Elsevier, 425 pp.

Sekine Y., 1988: On the seasonal variation in in- and outflow volume transport of the Japan Sea. *Progress in Oceanography*, Vol. 21, Pergamon, 269–279.

Teague W. J., and G. A. Jacobs, 2000: Current observations on the development of the Yellow Sea Warm Current. *J. Geophys. Res.*, **105** ((C2),), 3401–3411. Find this article online

Teague W. J., H. T. Perkins, Z. R. Hallock, and G. A. Jacobs, 1998: Current and tide observations in the southern Yellow Sea. *J. Geophys. Res.*, **103**, 27783–27793. Find this article online

Teague W. J., G. A. Jacobs, and J. W. Book, 2001: Tide observations in the Korea-Tsushima Strait. *Cont. Shelf Res.*, **21**, 545–561. Find this article online

Toba Y., K. Tomizawa, Y. Kurasawa, and K. Hanawa, 1982: Seasonal and year-to-year variability of the Tsushima–Tsugaru Warm Current system with its possible cause. *La Mer*, **20**, 41–51. Find this article online

Yi S. U., 1966: Seasonal and secular variations of the water volume transport across the Korea Strait. *J. Oceanol. Soc. Korea*, **1**, 7–13. Find this article online

Yi S. U., 1970: Variations of oceanic condition and mean sea level in the Korea Strait. *The Kuroshio: A Symposium on the Japan Current*, J. C. Marr, Ed., East-West Center Press, 125–141.

Tables

TABLE 1. ADCP summary

Mooring	Lat (°)	Lon (°)	Start day	End day	Top bin (m)	Bottom bin (m)	Bin size (m)	Water depth (m)
S1	34.32	127.90	130	289	5	53	2	59
			290	437	6	55	1	
S2	34.13	128.12	129	289	7	83	2	89
			290	438	7	83	2	
S3	33.93	128.34	129	288	11	103	4	113
			290	438	11	103	4	
S4	33.74	128.56	128	287	9	97	4	107
			288	438	9	97	4	
S5	33.54	128.78	128	287	19	143	4	152
S6	33.35	129.00	128	286	9	105	4	115
			288	438	9	105	4	
C1	34.95	129.26	292	444	7	97	2	103
K1	33.64	126.52	62	356	6	114	4	124
N1	35.31	129.60	293	440	9	113	4	119
N2	35.20	129.67	125	282	25	137	2	142
			285	441	24	132	4	
N3	35.01	129.99	126	283	13	125	4	132
			285	441	11	123	4	
N4	34.84	130.21	126	283	13	117	4	127
			285	441	13	117	4	
N5	34.67	130.43	127	284	16	120	4	130
			285	442	11	119	4	
N6	34.50	130.65	127	284	12	108	4	118
			286	442	12	108	4	

Click on thumbnail for full-sized image.

TABLE 2. Monthly mean transport (Sv) for 1999–2000

	May	Jun	Jul	Aug	Sep	Oct	Nov	Dec	Jan	Feb	Mar	Avg	σ
N line	1.9	2.1	2.3	2.9	2.8	3.2	3.3	1.9	1.6	1.6	2.3	2.3	0.62
S line	2.7	2.8	2.8	3.0	3.1	3.5	3.1	1.8	1.7	2.2	2.8	2.7	0.55

Click on thumbnail for full-sized image.

Figures

Click on thumbnail for full-sized image.

FIG. 1. ADCP mooring locations, and bathymetry. Depths are in meters. Cheju Strait is located between Cheju-Do and Korea. The Korea/Tsushima Strait is located between Japan and Korea. Bathymetry is from the 1999 Digital Atlas for Neighboring Seas of Korean Peninsula (provided by Prof. Byung-Ho-Choi, Laboratory for Coastal and Ocean Dynamics Studies, Sungkyunkwan University)

Click on thumbnail for full-sized image.

FIG. 2. Snapshots of the along-strait velocities for representative current configurations after tide removal are shown for the south section. The vertical axis is depth and the horizontal axis is along the section and across the Korea/Tsushima Strait from west to east. Positive velocities are toward the northeast

Click on thumbnail for full-sized image.

FIG. 3. As in Fig. 2 but for the north section

Click on thumbnail for full-sized image.

FIG. 4. Overall and monthly near-surface speed histograms. Vertical bars indicate the frequency of current observations occurring within 10 cm s^{-1} velocity bins after tides have been removed. Asterisks indicate the frequency of current observations that include tidal currents.

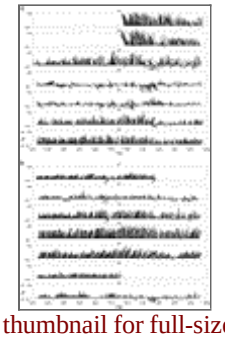

Click on thumbnail for full-sized image.

FIG. 5. (a) Vector stick diagrams of current velocities for ADCPs along the northern section, and C1. The currents have been vertically averaged for each ADCP. Tides have been removed using a low-pass filter with a 40-h cutoff frequency. *X*-axis units are in days beginning in 1999. (b) As in (a) but for the southern section, including mooring K1.

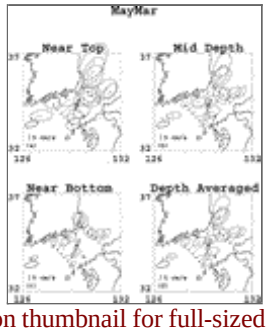

Click on thumbnail for full-sized image.

FIG. 6. Mean currents near the surface (top velocity bin) (a), for mid-depth currents (middle velocity bin) (b), for near-bottom currents (bottom velocity bin) (c), and for depth-averaged currents, (d) and their corresponding standard deviation ellipses after tide removal are shown for the 11-month period (May 1999–Oct 2000)

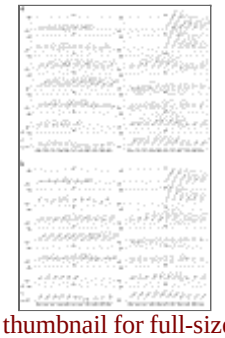

Click on thumbnail for full-sized image.

FIG. 7. Monthly time series of mean current vectors and their corresponding standard deviation ellipses for near-surface (top velocity bin) (a), mid-depth (b), and near-bottom (c) levels

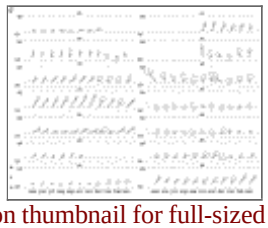

Click on thumbnail for full-sized image.

FIG. 7 (*Continued*)

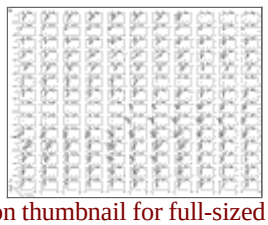

Click on thumbnail for full-sized image.

Click on thumbnail for full-sized image.

FIG. 8. Monthly mean velocity profiles (heavy line) and standard deviation (horizontal bars) for (a) the across-strait velocity (U_r) (approximately parallel to the north and south sections). The zero velocity is indicated by the light vertical line. (b) As in (a) but for the along-strait velocity (V_r) (approximately normal to the south and north sections).

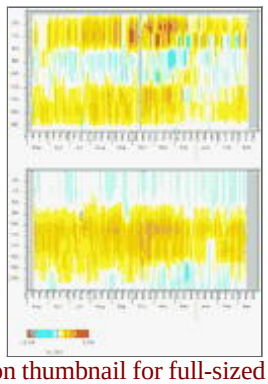

Click on thumbnail for full-sized image.

FIG. 9. Transport variability is indicated by the vertically integrated velocity as a function of distance (km) from Korea and time for the northeastern section (top) and southwestern section (bottom)

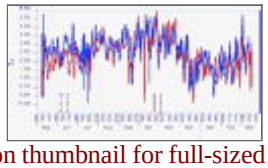

Click on thumbnail for full-sized image.

FIG. 10. Total transport estimates for the southwestern section (blue) and northeastern section (red) are shown as a function of time. The corresponding time-averaged transports are 2.7 Sv and 2.3 Sv. The rms transport error estimate is shown in the lower left by the confidence intervals. These error estimates are time-invariant

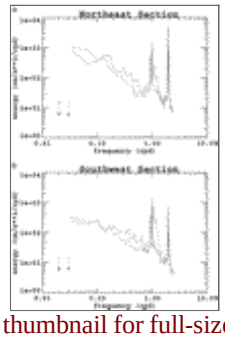

Click on thumbnail for full-sized image.

FIG. 11. Average energy spectra for moorings along the northeast (a) and southwest (b) sections for summer (solid line) and winter (dashed line). Confidence levels indicated by the vertical bars correspond to the 95% significance level

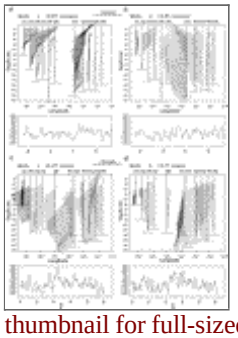

Click on thumbnail for full-sized image.

FIG. 12. EOF analyses of the moorings along both the northeast and southwest sections for (a) Mode 1 summer, (b) Mode 2 summer, (c) Mode 1 winter, and (d) Mode 2 winter. North is up along the *y* axis and east is to the right along the *x* axis. The vectors in the upper panels are scaled in time by the time series in the lower panels, and reverse direction on sign change by the time series. The vector velocity scale is indicated by the bar at the top of the figure. Horizontal bars at the bottom of each profile correspond to bottom depths

* Naval Research Laboratory/Stennis Space Center Contribution Number JA/7330/01/0067.

Corresponding author address: Mr. W. J. Teague, Meso- and Finescale Ocean Physics Section, Naval Research Laboratory, Stennis Space Center, MS 39529-5004. E-mail: Teague@nrlssc.navy.mil

top